Inorganic Chemistry

Article

pubs.acs.org/IC

Reactions of 11-Vertex Rhodathiaboranes with HCl: Synthesis and Reactivity of New Cl-Ligated Clusters

Beatriz Calvo,[†] Ramón Macías,*[,†] Maria Jose Artigas,[†] Fernando J. Lahoz,[†] and Luis A. Oro[†,‡]

[†]Departamento de Química Inorgánica, Instituto de Síntesis Química y Catálisis Homogénea, Universidad de Zaragoza-CSIC, 50009-Zaragoza, Spain

[‡]King Fahd University of Petroleum and Minerals, Dhahran 31261, Saudi Arabia

Supporting Information

ABSTRACT: Reactions of [8,8,8-(H)(PPh_3)$_2$-9-(Py)-*nido*-8,7-$RhSB_9H_9$] (**1**), [1,1-(PPh_3)$_2$-3-(Py)-*closo*-1,2-$RhSB_9H_8$] (**2**), and [1,1-(CO)(PPh_3)-3-(Py)-*closo*-1,2-$RhSB_9H_8$] (**4**), where Py = Pyridine, with HCl to give the Cl-ligated clusters, [8,8-(Cl)-(PPh_3)-9-(Py)-*nido*-8,7-$RhSB_9H_9$] (**3**) and [8,8,8-(Cl)(CO)(PPh_3)-9-(Py)-*nido*-8,7-$RhSB_9H_8$] (**5**), have recently demonstrated the remarkable *nido*-to-*closo* redox flexibility and bifunctional character of this class of 11-vertex rhodathiaboranes. To get a sense of the scope of this chemistry, we report here the reactions of PR_3-ligated analogues, [8,8,8-(H)(PR_3)$_2$-9-(Py)-*nido*-8,7-$RhSB_9H_9$], where PR_3 = $PMePh_2$ (**6**), or PPh_3 and PMe_3 (**7**); and [1,1-(PR_3)$_2$-3-(Py)-*closo*-1,2-$RhSB_9H_8$], where PR_3 = PPh_3 and PMe_3 (**8**), PMe_3 (**9**) or PMe_2Ph (**10**), with HCl to give Cl-ligated clusters. The results demonstrate that in contrast to the PPh_3-ligated compounds, **1**, **2**, and **3**, the reactions with **6**−**10** are less selective, giving rise to the formation of mixtures that contain monophosphine species, [8,8-(Cl)(PR_3)-9-(Py)-*nido*-8,7-$RhSB_9H_9$], where PR_3 = PMe_3 (**11**), PMe_2Ph (**12**), or $PMePh_2$ (**15**), and bis-ligated derivatives, [8,8,8-(Cl)(PR_3)$_2$-9-(Py)-*nido*-8,7-$RhSB_9H_9$], where PR_3 = PMe_3 (**13**) or PMe_2Ph (**14**). The {RhCl(PR_3)}-containing compounds, **3**, **11**, **12**, and **15**, are formally unsaturated 12 skeletal electron pair (sep) clusters with *nido*-structures. Density functional theory (DFT) calculations demonstrate that the *nido*-structure is more stable than the predicted *closo*-isomers. In addition, studies have been carried out that involve the reactivity of **3** with Lewis bases. Thus, it is reported that **3** interacts with MeCN in solution, and it reacts with CO and pyridine to give the corresponding Rh-L adducts, [8,8,8-(Cl)(L)(PPh_3)-9-(Py)-*nido*-8,7-$RhSB_9H_9$], where L = CO (**5**) or Py (**20**). On the other hand, the treatment of **3** and **5** with Proton Sponge (PS) promotes the abstraction of HCl, as [PSH]Cl, from the *nido*-clusters, and the regeneration of the parent *closo*-species, completing two new stoichiometric cycles that are driven by Brønsted acid/base chemistry.

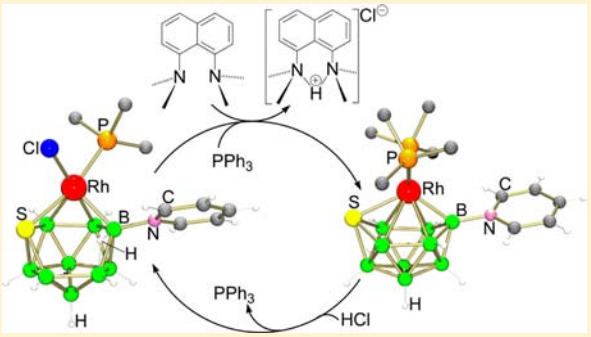

INTRODUCTION

In polyhedral boron chemistry, it has long been a goal to develop catalytic cycles by combining the oxidative and coordinative richness of transition metal elements with the capability of boron clusters to exhibit oxidative/reductive flexibility in their classical *closo-nido-arachno* transformations. In this regard, we have shown that the 11-vertex rhodathiaborane system, [8,8,8-(H)(PPh_3)$_2$-9-(Py)-*nido*-8,7-$RhSB_9H_9$] (**1**)/[1,1-(PPh_3)$_2$-3-(Py)-*closo*-1,2-$RhSB_9H_8$] (**2**) exhibits a remarkable *nido*-to-*closo* redox reactivity that can operate in the hydrogenation of alkenes (Py = pyridine).[1] In this system, the {SB_9H_8(Py)} fragment can be regarded as a non-innocent ligand that cooperates with the metal vertex in the reactions, conferring a bifunctional nature to these rhodathiaboranes.

Reactions of **1** and **2** with hydrochloric acid have recently demonstrated further the remarkable lability and bifunctional character of these 11-vertex rhodathiaboranes.[2] These reactions are new convenient routes to Cl-ligated rhodathiaboranes; thus, air-stable yellow [8,8-(Cl)(PPh_3)-9-(Py)-*nido*-8,7-$RhSB_9H_9$] (**3**) can be synthesized in high yield from [RhCl(PPh_3)$_3$] and readily available Cs[*arachno*-6-SB_9H_{12}], carrying out three steps (Scheme 1).

Alternatively, compound **3** can be prepared in 75% yield from the reaction of the *closo*-derivative, **2**, with HCl. Similarly, the CO-ligated counterpart, [1,1-(CO)(PPh_3)-9-(Py)-*closo*-1,2-$RhSB_9H_8$] (**4**), reacts with HCl to give orange-yellow [8,8,8-(Cl)(CO)(PPh_3)-9-(Py)-*nido*-8,7-$RhSB_9H_9$] (**5**). Building upon the reactivity of **1** and **2** with hydrochloric acid, we have extended our studies to the PR_3-ligated analogues, [8,8,8-(H)(PR_3)$_2$-9-(Py)-*nido*-8,7-$RhSB_9H_9$], where PR_3 = $PMePh_2$ (**6**), or PPh_3 and PMe_3 (**7**);[3] and [1,1-(PR_3)$_2$-3-(Py)-*closo*-1,2-$RhSB_9H_8$], where PR_3 = PPh_3 and PMe_3 (**8**), PMe_3 (**9**) or PMe_2Ph (**10**),[3] discussing trends and differences within this family of 11-vertex clusters.

Received: August 3, 2012
Published: December 10, 2012

   dx.doi.org/10.1021/ic301715n | *Inorg. Chem.* 2013, 52, 211−221

Scheme 1. Synthesis of 3

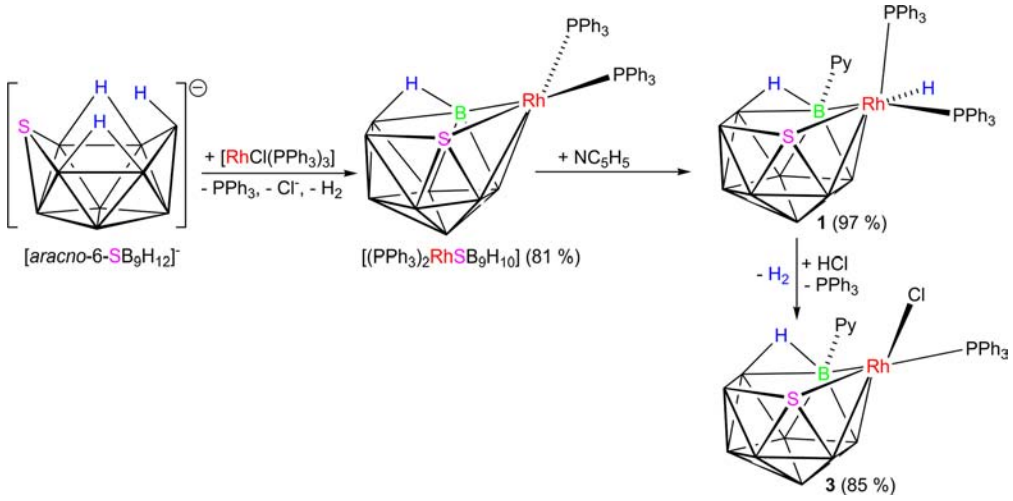

Scheme 2

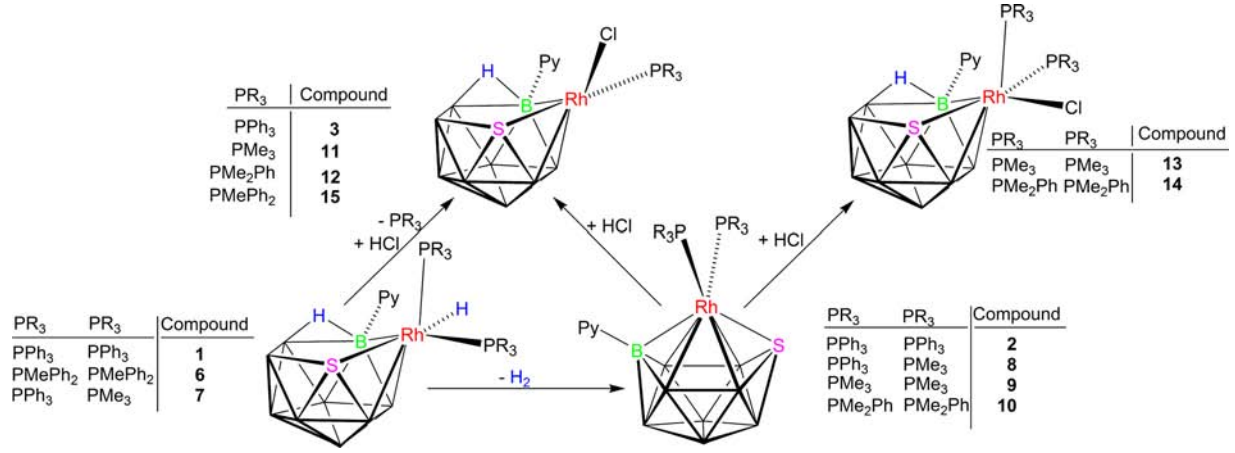

RESULTS AND DISCUSSION

Reactions of *closo*- and *nido*-Rhodathiaboranes with HCl. Scheme 2 can be used as a guide to the following sections. The synthesis of **3** and its reactivity with CO has been described earlier.[2] Now we explore the reactivity of the 11-vertex *nido*- and *closo*-rhodathioaboranes, **6**−**10**, which are PR_3-ligated derivatives of the *nido*- and *closo*-counterparts, **1** and **2**. As commented in the introduction, the treatment of the *closo*-derivative, **2**, with aqueous HCl, followed by filtration and drying over magnesium sulfate, affords **3** in good yields (Scheme 1).[2] Similarly, the reactions of the *bis*-PR_3-ligated *closo*-counterparts, **9** and **10**, with HCl yield new monophosphine *nido*-clusters, [8,8-(Cl)(PR_3)-9-(Py)-*nido*-8,7-$RhSB_9H_9$], where PR_3 = PMe_3 (**11**) or PMe_2Ph (**12**), in moderate to high yields. However, when these reactions were carried out on small scale in NMR tubes, the solvent was evaporated and the resulting residue washed with hexane, the NMR data showed the formation of mixtures that contained the monophosphine-ligated clusters, **11** and **12**, together with the bis-phosphine derivatives, [8,8,8-(Cl)(PR_3)$_2$-9-(Py)-*nido*-8,7-$RhSB_9H_9$], where PR_3 = PMe_3 (**13**), PMe_2Ph (**14**), with higher ratios of the bis-phosphine to the monophosphine compounds.

In contrast to **9** and **10**, the reaction of the mixed PR_3-ligated analogue **8** with HCl affords a mixture of **3** and **11** in a 1:2 ratio. Alternatively, **3** is also available from the reaction of **1** and hydrochloric acid;[2] likewise, the treatment of the *nido*-hydridorhodathiaboranes, [8,8,8-(H)(PR_3)$_2$-9-(Py)-*nido*-8,7-$RhSB_9H_9$], where PR_3 = $PMePh_2$ (**6**), or PPh_3 and PMe_3 (**7**), with HCl affords the corresponding chloro-derivatives, [8,8-(Cl)(PR_3)-9-(Py)-*nido*-8,7-$RhSB_9H_9$], where PR_3 = PMe_3 (**11**) or $PMePh_2$ (**15**).

Structural Aspects. The structures of **3** and **5** were reported in an earlier communication,[2] and now these are analyzed in more detail, together with the new Cl-ligated clusters, [8,8,8-(Cl)(PMe_3)$_2$-9-(Py)-*nido*-8,7-$RhSB_9H_9$] (**13**) and [8,8,8-(Cl)-(PMe_2Ph)$_2$-9-(Py)-*nido*-8,7-$RhSB_9H_9$] (**14**). It should be noticed that for **13** a static disorder was observed in the thiaborane fragment and the phosphine ligands. This disorder has been modeled with two sets of positions with complementary occupancy factors (0.92/0.08). The distances and angles discussed below deal with the major occupancy cluster.

These compounds have a *nido* 11-vertex cluster geometry with a five-membered {$RhSB_3$} open face (schematic II, Figure 1). This structure is now well represented with examples that show different combinations of *exo*-polyhedral ligands either at the B(9) vertex or at the Rh(8) center. In compound **3**, the pentagonal open face has a pyridine-bound vertex at the B(9) position and a {Rh(Cl)(PPh_3)} fragment, which renders this

dx.doi.org/10.1021/ic301715n | Inorg. Chem. 2013, 52, 211−221

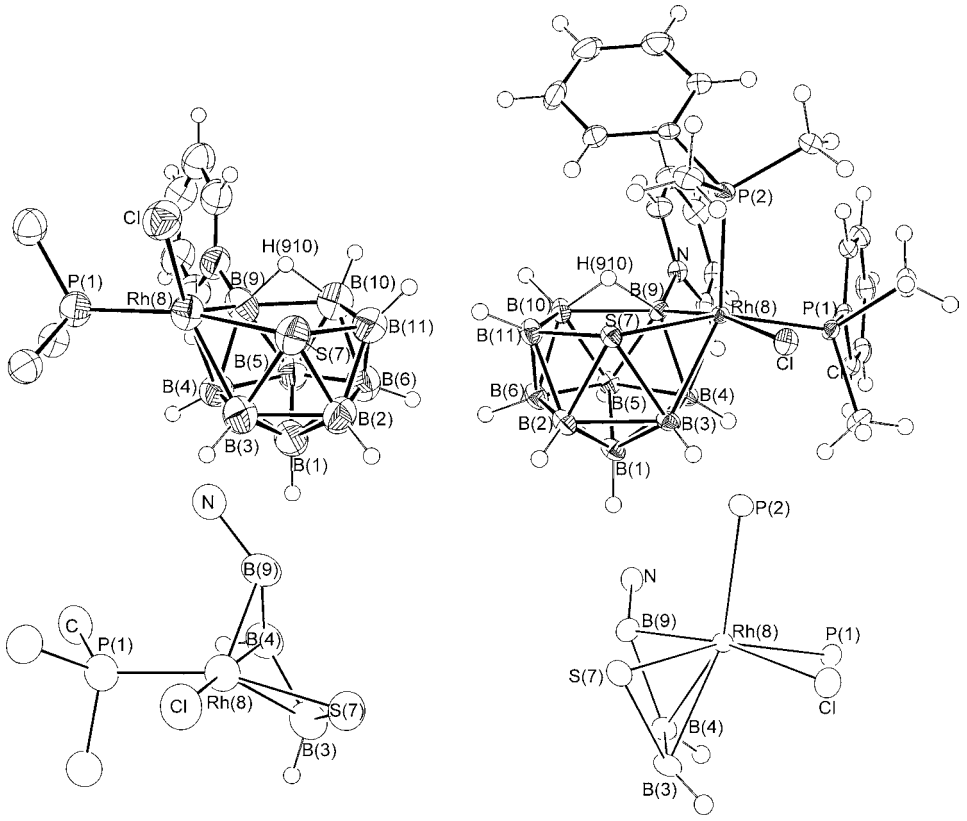

Figure 1. ORTEP-type of drawing of compounds **3** (left) and **14** (right), and detail of the rhodium-to-cluster coordination sphere (below the clusters). Ellipsoids are shown at 50% probability levels.

cluster isoelectronic with [8,8-$(L)_2$-*nido*-8,7-$RhSB_9H_{10}$], where L = PPh_3 (**16**),[4] $(CH_2)_3(PPh_2)_2$,:[5] rhodathiaboranes that exhibit a B(9)−H(9) vertex and {RhP_2} fragments as part of the open face (schematic cluster structure I).

Compounds **5**, **13**, and **14** are based on the same pyridine-substituted {η^4-SB_9H_9(Py)} fragment than **3**, but with rhodium vertices that bear a third *exo*-polyhedral ligand to form the organometallic fragments, {Rh(Cl)(CO)(PPh_3)}, {Rh(Cl)-(PMe_3)$_2$}, and {Rh(Cl)(PMe_2Ph)$_2$}, respectively (schematic cluster structure II, Figure 1). These rhodium units are reminiscent of **1**,[6] which contains a {Rh(H)(PPh_3)$_2$} fragment at the 8-position. Thus, for comparison, important interatomic distances and angles in **1**, **3**, **5**, **13**, and **14** are given in Table 2.

A common structural feature of **3** and **16** is that the {RhCl(PPh_3)} and {Rh(PPh_3)$_2$} units are twisted away from a reference plane through Rh(8)B(1)B(6). The dihedral angles Φ between the planes formed by P(1)Rh(8)Cl and P(1)-Rh(8)P(2), in **3** and **16**, and the S(7)Rh(8)B(9) plane are 53° and 59°, respectively. Table 1 gathers this structural facet that is found in 11-vertex metallaheteroboranes that incorporate {M(L)$_2$}- and {MClL}-fragments, where M = Rh, Ir, or Pt. Also listed in Table 1 are the angles between the {M(8)E(7)-B(9)} and {E(7)B(2)B(5)B(9)}, where E = C, N, or S, planes in different 11-vertex metallaheteroboranes (Figure 2). This dimension is appropriate to examine for intermediacy of structure between conventionally *nido* compounds **1**, **3**, **5**, **6**, **13**, and **14**, and *closo*-cages **2**, **8**, **9**, and **10**. The data indicate that conventional *nido*-structures exhibit a θ angle close to 50°, whereas, in 11-vertex metallaheteroboranes that incorporate {ML_2} units, there is some shift from the *nido* structure toward the closed octadecahedral cage. As expected for 11-vertex *isonido*-clusters, which exhibit a quadrilateral open face, the θ angles are closer to pure 11-vertex octadodecahedral *closo*-cages than to 11-vertex icosahedral *nido*-clusters, but clearly shifted toward the *nido*-cage when compared to typical 11-vertex *closo*-cages (see Table 1).

The {RhCl(PPh_3)} unit is an unusual moiety in rhodaheteroboranes, which, within the polyhedral environment of a {η^4-SB_9}-to-Rh interaction as in **3**, has only been crystallographically characterized in the dirhodadithiaborane, [$(PPh_3)_2HRh(PPh_3)ClRhS_2B_7H_7$] (**17**; schematic cluster structure III).[16] A similar rhodium-to-thiaborane interaction is found in [8-Cl-{8,9-(μ-dppm)}-10-PPh_3-*nido*-8,7-$RhSB_9H_7$] (**18**),[17] in which a diphenylphosphinemethane ligand, dppm, is bridging the Rh(8) atom and the 9-position in the open face of the cage (Schematics IV). The chlorine atom in **3** is attached to the rhodium center at a distance of 2.354(2) Å, which is shorter than the rhodium−chlorine bonds, 2.3710(10) and 2.370(2) Å, in **17** and **18**, respectively, but close to the value of 2.356(2) Å found in [2,3-$(PPh_3)_2$-3-Cl-μ-2;3-Cl-2-($Ph_2PC_6H_4$)-*closo*-2,3,1-$Rh_2SB_9H_8$].[4] In the bis-PR_3-ligated clusters, **13** and **14**, the Rh−Cl distance is markedly longer at 2.5196(7) and 2.5116(8) Å, respectively (the mean of Rh−Cl distances found in the CSD is 2.403(3) Å). It is interesting to point out that in the herein crystallographycally studied Cl-ligated clusters, **3**, **5**, **13**, and **14**, and other previously reported Cl-ligated rhodathiaboranes, the chlorine ligand is *trans* to boron vertices, contrasting with the preference of the hydride ligand to lie *trans* to the sulfur vertex (vide infra).

Comparative NMR Studies. The monophosphine-ligated 11-vertex rhodathiaboranes, **3**, **11**, **12**, and **15**, have been characterized by multinuclear NMR spectroscopy. The ^{11}B-

dx.doi.org/10.1021/ic301715n | *Inorg. Chem.* 2013, 52, 211−221

Table 1. Angles Φ and θ for 11-Vertex Metallaheteroboranes

compound	Φ[a]	θ[b]	ref
[8,8-$(PPh_3)_2$-*nido*-8,7-$RhSB_9H_{10}$] (**16**)	59°	46°	4
[8,8-$(PPh_3)_2$-9-(OEt)-*nido*-8,7-$RhSB_9H_9$]	63°	48°	7
[8,8-(η^2-dppe)-*nido*-8,7-$RhSB_9H_{10}$]	69°	48°	8
[8,8-(η^2-dppp)-*nido*-8,7-$RhSB_9H_{10}$]	69°	47°	5
[8,8-(η^2-dppp)-9-(OEt)-*nido*-8,7-$RhSB_9H_9$]	77°	46°	5
[8,8-(Cl)(PPh_3)-9-(Py)-*nido*-8,7-$RhSB_9H_9$] (**3**)	53°	49°	2
[1,1-$(PPh_3)_2$-3-(Py)-*closo*-1,2-$RhSB_9H_8$] (**2**)	85°	2°	6
[1,1-$(PMe_2Ph)_2$-3-(Py)-*closo*-1,2-$RhSB_9H_8$] (**10**)	83°	6°	3
[1,1-$(PMe_3)(PPh_3)$-3-(Py)-*closo*-1,2-$RhSB_9H_8$] (**8**)	85°	2°	3
[1,1,1-(H)$(PMe_3)_2$-*isonido*-1,2-$IrSB_9H_9$]	81°	13°	9
[1,1,1-(H)$(PPh_3)_2$-*isonido*-1,2-$IrC_2B_8H_{10}$]	88°	14°	10
[8,8-$(PPh_3)_2$-*nido*-8,7-$RhNB_9H_{11}$]	31°	38°	11
[8,8-$(PMe_2Ph)_2$-*nido*-8,7-$PtCB_9H_{11}$]	36°	37°	12
[8,8-$(PMe_2Ph)_2$-9-(OMe)-*nido*-8,7-$PtCB_9H_{10}$]	44°	36°	11
[8,8,8-(H)$(PPh_3)_2$-9-(Py)-*nido*-8,7-$RhSB_9H_9$] (**1**)		52°	1b
[8,8,8-(H)$(PMePh_2)_2$-9-(Py)-*nido*-8,7-$RhSB_9H_9$] (**6**)		50°	3
[8,8,8-(Cl)(CO)(PPh_3)-9-(Py)-*nido*-8,7-$RhSB_9H_9$] (**5**)		50°	2
[8,8,8-(Cl)$(PMe_2Ph)_2$-9-(Py)-*nido*-8,7-$RhSB_9H_9$] (**14**)	51°	this work	
[8,8,8-(CO)(η^2-dppe)-*nido*-8,7-$RhSB_9H_{10}$]		50°	13
[8,8,8-(η^2-dppe)(NCMe)-*nido*-8,7-$RhSB_9H_{10}$]		50°	13
[8,8,8-$(PMe_2Ph)_3$-*nido*-8,7-$RhSB_9H_{10}$]		50°	14
[8,8,8-(η^1-dppm)(η^2-dppm)-*nido*-8,7-$RhSB_9H_{10}$]		50°	5
[8,8,8-(k^2-bpy)(PPh_3)-*nido*-8,7-$RhSB_9H_{10}$]		52°	15
[8,8,8-(CO)$(PMe_3)_2$-*nido*-8,7-$IrSB_9H_{10}$]		51°	9

[a]Dihedral angles between {L(1)M(8)L(2)} and {E(7)M(8)B(9)} planes. [b]Dihedral angles between{M(8)E(7)B(9)} and {E(7)B(2)-B(5)B(9)}. *Nido* numbering is used to define the planes.

{^{1}H} NMR spectra show seven resonances in a 2:2:1:1:1:1:1 relative intensity ratio for **3**, **12** and **15**, whereas for the PMe_3-ligated analogue **11**, there are eight signals in the ratio 2:1:1:1:1:1:1:1, indicating that the clusters are asymmetric in solution (Figure 3). This asymmetry is further confirmed by the ^{1}H-{^{11}B} spectra that exhibit nine proton resonances of hydrogen atoms bound to boron atoms, resolving, therefore, the peaks of intensity two that correspond to overlapping ^{11}B resonances. The similarity of the ^{11}B NMR spectra in this series of Cl-ligated 11-vertex rhodathiaboranes is remarkable, suggesting that the substitution of PPh_3 in the crystallographically determined cluster, **3**, by the more basic phosphines, PMe_3, PMe_2Ph, and $PMePPh_2$, does not have a significant effect in the electronic distribution within the {η^4-$SB_9H_9(Py)$} moiety.

The four chloro-ligated clusters, **3**, **11**, **12**, and **15**, exhibit a sharp doublet in the corresponding ^{31}P-{^{1}H} NMR spectra at room temperature. This sharpness suggests that ^{31}P−^{11}B coupling is small, supporting an *exo*-polyhedral ligand orientation with the PR_3 ligands lying *trans* to the S(7) vertex. Thus, the {$Rh(Cl)PR_3$}-to-{η^4-$SB_9H_9(Py)$}, where PR_3 = PMe_3, PMe_2Ph, $PMePPh_2$, or PPh_3, configuration in solution appears to resemble that found in the solid state for **3** (Figure 1). The ^{31}P resonances shift from the low-field value of δ +32.2 in **3**, through the values of δ +18.1 and +12.3 in **15** and **12**, respectively, to the high-field resonance of δ +7.8 in **11**. The $^1J(^{103}Rh-^{31}P)$ coupling constant is 8 Hz smaller in the PMe_3-ligated cluster, **11**, than in the PPh_3 analogue **3**.

The bis-phosphine-ligated clusters, **13** and **14**, were characterized in situ by NMR in samples that contained the monophosphine parent species, **11** and **12**, as minor components. Although the assignment of the resonances has some ambiguity because of overlapping peaks, the ^{1}H-{^{11}B} and ^{11}B NMR data indicate that the pattern of the spectra do not change significantly upon coordination of a second phosphine ligand at the rhodium center (Figure 5 below). The ^{31}P-{^{1}H} spectra exhibit two principal resonances, which correspond to two different phosphine ligands. It is noteworthy that the highest field peak is broad in both species even at low temperature.

Bonding Considerations. Application of the electron-counting rules to compounds **3**, **11**, **12**, and **15** gives a formal 12 sep. This number predicts a *closo*-structure based on an octadodecahedon.[18] In compound **3**, the rhodium center could be tentatively described as having a distorted square-planar environment, with bonding vectors directed toward the two *exo*-polyhedral ligands, and the S(7) and B(4) vertices of the {$SB_9H_9(Py)$}-fragment, which in **3** are situated *trans* to the PPh_3 and Cl ligands, respectively (Figure 1).

A discrepancy between the electron-counting rules and the structure is common among polyhedral molecules that incorporate C_{2v} fragments such as {RhL_2} or {PtL_2}. This problem has been long recognized and rationalized,[19] and it has been dealt with in the literature several times.[11,16,20] Alternatively, it has been suggested[13] that two CH···Rh agostic interactions with two *ortho*-C-H bonds of the PPh_3 ligands of the {$Rh(PPh_3)_2$} unit in the formally unsaturated 11-vertex rhodathiaborane, **16**, play an important and decisive role in the stabilization of *nido* versus *closo* geometries in this type of compound. Incidentally, there are two CH···Rh contacts at 2.75 and 3.27 Å in the molecular structure of **3**, which could stabilize the *nido*-stucture by providing the additional electron pair to the cluster framework. To evaluate this hypothesis, we decided to undertake DFT calculations on the PH_3 model, [8,8-(Cl)(PH_3)-9-(Py)-*nido*-8,7-$RhSB_9H_9$] (**3a**), and its hydrido isomer [1,1,1-(Cl)(H)(PH_3)-3-(Py)-*isonido*-8,7-$RhSB_9H_8$] (**3b** and **3c**). The calculated structural and nuclear shielding properties of **3a** agree well with the experimental data of the Cl-ligated *nido*-clusters, **3**, **11**, **12**, and **15** (see Supporting Information, Table S1) suggesting that **3a** is a reasonable model for these 11-vertex unsaturated clusters. The energy of the optimized minima for the *nido*-isomer, **3a**, lies 57 kJ/mol lower in energy than the isomer **3b** (Figure 4) which exhibits an *isonido*-structure. This structure, with a {Rh(1)S(2)B(4)B(7)} quadrilateral open face, resembles calculated intermediates along the fluxional pathway of compound **16**[11] as well as the crystallographically determined hydridoiridathiaborane, [1,1,1-(H)$(PMe_3)_2$-*isonido*-1,2-$IrSB_9H_9$] (**19**).[9] It is interesting to note that a {η^4-$SB_9H_8(Py)$}-to-{$Rh(Cl)(H)(PH_3)$} conformational change from **3b** to **3c** implies an increase of 50 kJ/mol in the energy of the PH_3-model, indicating that there is a clear preference of the hydride ligand to occupy the position *trans* to the sulfur vertex versus to a boron vertex of the hexagonal {S(1)B(3)B(4)B(5)B(6)B(7)} face. Since the boron vertex in metallaheteroboranes has a stronger *trans* influence than the cage heteroatoms,[21] the final *exo*-polyhedral orientation of the metal ligands with respect to the {$SB_9H_8(Py)$} fragment is controlled by the sulfur vertex with the hydride ligand, which have a stronger *trans* influence than chlorine and PR_3 ligands, lying *trans* to the cage S atom. This effect, therefore, stabilizes the calculated *isonido*-conformer **3b** versus **3c**; however it is not

dx.doi.org/10.1021/ic301715n | *Inorg. Chem.* 2013, 52, 211−221

Table 2. Selected Interatomic Distances (Å) for [8,8,8-(H)$(PPh_3)_2$-9-(Py)-*nido*-8,7-$RhSB_9H_9$] 1, [8,8,8-(Cl)(PPh_3)-9-(Py)-*nido*-8,7-$RhSB_9H_9$] 3, [8,8,8-(Cl)(CO)(PPh_3)-9-(Py)-*nido*-8,7-$RhSB_9H_9$] 5 [8,8,8-(Cl)$(PMe_3)_2$-9-(Py)-*nido*-8,7-$RhSB_9H_9$] 13, [8,8,8-(Cl)$(PMe_2Ph)_2$-9-(Py)-*nido*-8,7-$RhSB_9H_9$] 14, and [8,8-$(PPh_3)_2$-*nido*-8,7-$RhSB_9H_{10}$] 16

	1	3	5	13	14	16
Rh(8)−S(7)	2.431(2)	2.361(2)	2.4060(16)	2.3654(7)	2.3574(7)	2.3769(12)
Rh(8)−P(1)	2.354(2)	2.294(2)	2.4091(7)	2.2830(6)	2.2990(7)	2.2906(11)
Rh(8)−P(2)	2.341(2)			2.3635(7)	2.3868(7)	2.4198(11)
Rh(8)−H(1)	1.54(6)					
Rh(8)−Cl(1)		2.354(2)	2.4295(9)	2.5196(6)	2.5116(8)	
Rh(8)−B(9)	2.220(9)	2.099(8)	2.211(2)	2.166(2)	2.179(3)	2.145(4)
Rh(8)−B(3)	2.201(11)	2.202(10)	2.206(18)	2.270(9)	2.230(3)	2.243(4)
Rh(8)−B(4)	2.217(10)	2.198(9)	2.223(4)	2.211(2)	2.218(3)	2.236(4)
Rh(8)−C(1)			1.833(3)			
C(1)−O(1)			1.130(5)			
B(9)−N(1)	1.547(11)	1.548(12)	1.546(3)	1.566(2)	1.566(4)	
S(7)−B(2)	1.980(9)	1.975(10)	1.970(3)	1.995(2)	1.985(3)	1.986(5)
S(7)−B(3)	2.059(11)	2.056(9)	2.07(2)	2.073(9)	2.102(3)	2.035(4)
S(7)−B(11)	1.953(9)	1.909(6)	1.899(10)	1.914(2)	1.914(3)	1.908(5)
B(2)−B(3)	1.906(14)	1.886(14)	1.964(19)	1.893(9)	1.925(5)	1.886(6)
B(3)−B(4)	1.772(15)	1.799(13)	1.788(17)	1.798(9)	1.800(5)	1.766(5)
B(2)−B(6)	1.745(14)	1.776(14)	1.756(4)	1.746(3)	1.758(5)	1.744(7)
B(4)−B(9)	1.819(16)	1.791(13)	1.807(5)	1.809(3)	1.786(4)	1.785(5)
B(9)−B(10)	1.856(13)	1.847(14)	1.825(4)	1.880(3)	1.898(4)	1.864(6)
B(10)−B(11)	1.784(14)	1.894(14)	1.817(4)	1.805(3)	1.808(5)	1.863(7)
P(1)−Rh(8)−C(1)			86.63(11)			
P(1)−Rh(8)−P(2)	100.27(7)			95.96(2)	101.88(3)	98.50(3)
P(1)−Rh(8)−H(1)	71(2)					
P(2)−Rh(8)−H(1)	98(2)					
P(1)−Rh(8)−Cl(1)		90.62(7)	92.08(2)	82.91(2)	83.08(2)	
P(2)−Rh(8)−Cl(1)				91.13(2)	84.29(2)	
P(1)−Rh(8)−S(7)	96.38(7)	163.83(7)	93.95(4)	163.30(2)	160.88(3)	170.05(4)
P(2)−Rh(8)−S(7)	102.05(8)			94.98(2)	91.85(2)	85.88(3)
P(1)−Rh(8)−B(4)	114.3(3)	92.9(2)	128.67(9)	89.62(6)	85.74(8)	89.46(10)
P(1)−Rh(8)−B(9)	162.4(3)	102.0(3)	175.97(6)	102.04(5)	100.96(8)	93.08(10)
S(7)−Rh(8)−Cl(1)		87.4(4)	86.73(7)	84.31(2)	85.15(2)	
Cl(1)−Rh(8)−B(4)		176.1(2)	139.16(9)	122.44(6)	123.71(9)	
Cl(1)−Rh(8)−B(9)		128.2(3)	91.30(7)	169.26(5)	169.69(8)	
B(9)−Rh(8)−S(7)	87.1(3)	92.1(3)	88.37(7)	84.91(5)	88.36(8)	92.30(11)
Cl(1)−Rh(8)−C(1)			105.48(11)			
Rh(8)−B(9)−N(1)	120.6(5)	120.60(6)	117.22(15)	126.17(12)	126.7(2)	

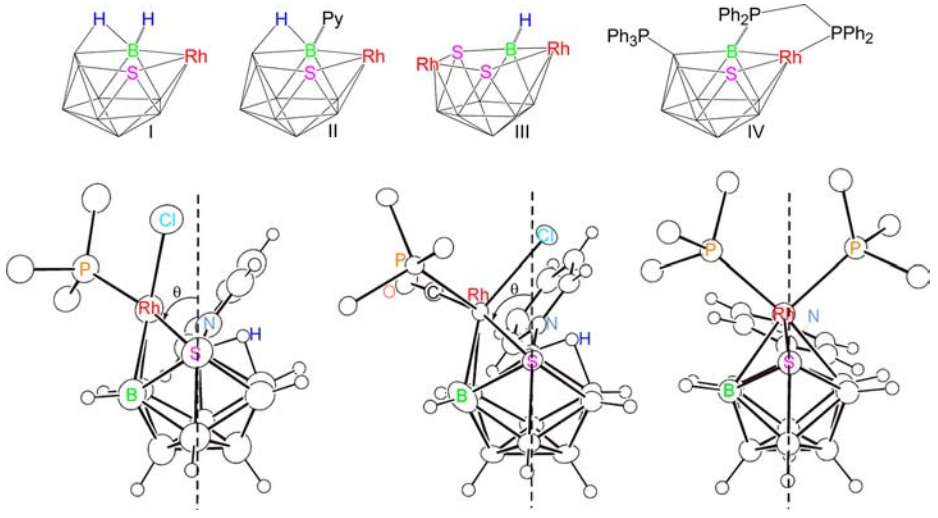

Figure 2. Drawings of compounds **3**, **5**, and **2**, respectively, illustrating the angle θ between the {Rh(8)S(7)B(9)} and {S(7)B(2)B(5)B(9)}, which is virtually zero for the 11-vertex octadecahedral *closo*-structure of **2**, and 50° for the *nido*-cages of **3** and **5**. For an 11-vertex fragment of a regular icosahedron it would be 62°.

dx.doi.org/10.1021/ic301715n | *Inorg. Chem.* 2013, 52, 211−221

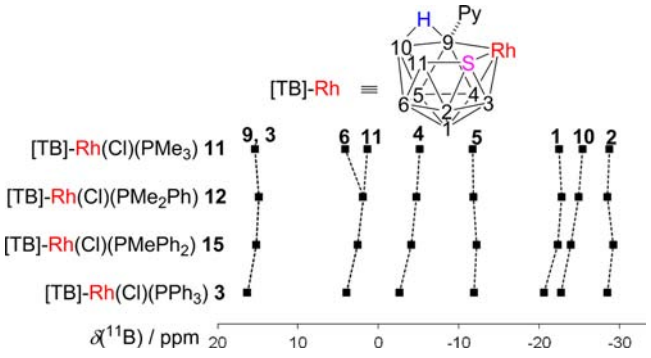

Figure 3. Diagrams representing the chemical shifts in the ^{11}B NMR spectra. Hatched lines connect equivalent positions. Assignments were made based on ^{1}H-{^{11}B(sel)} experiments and DFT-calculations on the PH_3 model, [8,8-(Cl)(PH_3)-9-(Py)-*nido*-8,7-$RhSB_9H_9$] (**3a**).

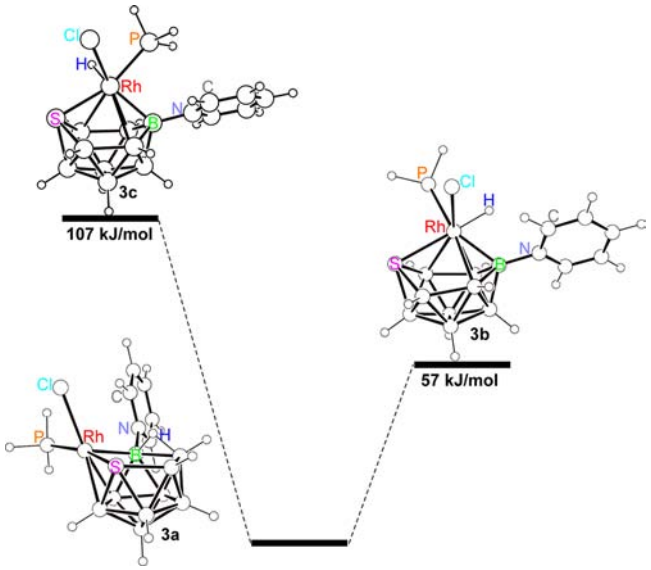

Figure 4. DFT-calculated energies and structures, computed at the B3LYP/6-31G*/LANL2DZ level for the PH_3 model [8,8-(Cl)(PH_3)-9-(Py)-*nido*-8,7-$RhSB_9H_9$] (**3a**) and two rhodium-hydride ligated isomers, [1,1-(Cl)(H)(PH_3)-3-(Py)-*isonido*-8,7-$RhSB_9H_8$] (**3b** and **3c**).

strong enough to stabilize the *isonido* structure versus the *nido*; in other words, in **3** a B−H−B bridging position for the hydrogen atom is more stable than the formation of a Rh−H bond *trans* to the sulfur vertex. This contrasts with compound **19** in which an 11-vertex *isonido*-structure with a S(2)-to-{Ir(1)H} *trans* configuration is more stable than the B−H−B *nido*-isomer.[9] In this regard, a boron vertex-to-metal hydride destabilizing effect is also directing the exopolyhedral ligand orientation in the previously reported hydridometallathiaboranes [8,8,8-(H)(PR_3)$_2$-9-(Py)-*nido*-8,7-$RhSB_9H_9$], where PR_3 = PPh_3 (**1**),[1a] $PMePh_2$ (**6**),[3] [8,8,8-(H)($PMePh_2$)$_2$-9-($PMePh_2$)-*nido*-8,7-$RhSB_9H_9$],[3] [8,8,8-(H)(PPh_3)$_2$-*nido*-8,7-$RhS_2B_8H_8$],[22] [8,8,8-(H)(PPh_3)$_2$-*nido*-8,7-$RhCSB_8H_{10}$],[23] [8,8,8-(H)(PPh_3)$_2$-*nido*-8,7,12-$IrS_2B_9H_9$],[22] [2,2,2-(H)(PMe_3)$_2$-*nido*-2,6-$IrSB_8H_{10}$],[24] and [2,2,2-(H)(PMe_3)$_2$-*closo*-2,1-$IrSB_8H_8$],[24] in which invariably the hydride ligand lies *trans* to the sulfur vertex.

In conclusion, the calculations presented here for the Cl-ligated species, with PH_3 ligands, demonstrate that the *nido* structure is more stable in the ground state, that is, as isolated molecules. Therefore, without any possible contribution from *agostic* interactions from P-aryl hydrogen atoms or from other molecules, there is no need to invoke CH···Rh agostic interactions to account for the molecular structures of **3**, **11**, **12**, and **15**. These results conform to analogous DFT analysis performed on the isoelectronic 11-vertex rhodathiaborane, [8,8-(PPh_3)$_2$-*nido*-8,7-$RhSB_9H_{10}$] (**16**).[11]

Reactions with Lewis Bases. The electronic unsaturation of the 11-vertex Cl-ligated rhodathiaboranes augurs a rich reaction chemistry with Lewis bases. The following sections describe the interaction of **3** with CH_3CN, and the reactions with CO, pyridine, and Proton Sponge.

As illustrated in Supporting Information, Figures S10 to S12, the addition of 8 equiv of acetonitrile to a solution of **3** in dichloromethane results in significant changes of the NMR spectra. Thus, ^{11}B resonances corresponding to the B(9), B(3), and B(5) vertices shift toward high field, the B(6) and B(11) peaks, which overlap in CD_2Cl_2 (top trace of Supporting Information, Figure S10), split upon addition of CH_3CN to separate clearly in neat CD_3CN (bottom trace of Supporting Information, Figure S10), whereas the peaks corresponding to B(1) and B(10) overlap to split again in neat CD_3CN. Changes are also significant in the ^{1}H resonances of the boron-bound hydrogen atoms (Supporting Information, Figure S11). The effect is clear in the high field shift of the H(1), H(3), H(10), and μ-H(9,10) proton resonances, whereas those corresponding to H(4), H(5), H(6), and H(11) appear to approach to each other, suffering a shielding. Finally, the ^{31}P-{^{1}H} spectrum exhibits a slight shift of the sharp doublet to low fields, and a change of the $^{1}J(^{103}Rh-^{31}P)$ coupling constant from 153 Hz in CD_2Cl_2 to 140 Hz in CD_3CN (Supporting Information, Figure S12).

In addition to the above-noted changes, in neat CD_3CN, there is formation of minor species, inferred from new low intensity peaks in the ^{11}B-{^{1}H}NMR spectrum and the existence of a new broad peak at +15.0 ppm in the ^{31}P-{^{1}H} spectrum. Interestingly, when the sample is evaporated to dryness and dissolved in CD_2Cl_2, the NMR spectra correspond to the Cl-ligated cluster, **3**, demonstrating that the behavior in acetonitrile is reversible.

These results are consistent with the existence of an equilibrium between **3**, free acetonitrile, and a CH_3CN-ligated species of formulation [8,8,8-(Cl)($NCCH_3$)(PPh_3)-9-(Py)-*nido*-8,7-$RhSB_9H_9$], with the equilibrium shifted to the left of eq 1 below. Under this rationale, the low intensity NMR resonances found in the ^{11}B-{^{1}H} and ^{31}P-{^{1}H} spectra in CD_3CN (Supporting Information, Figures S10 to S12) should correspond to the acetonitrile adduct, which upon evaporation of the solvent gives **3**.

$$\mathbf{3} + CH_3CN \rightleftharpoons [(Cl)(NCCH_3)(PPh_3)(Py)RhSB_9H_9] \quad (1)$$

PGSE NMR diffusion experiments reveal that the self-diffusion coefficient, *D*, of free acetonitrile (10 mM) in CD_2Cl_2 at 300 K, changes from a value of 3.73×10^{-9} m^2/s to 3.26×10^{-9} m^2/s when the chloro-derivative, **3**, is added to give a mixture of 4:1 ratio of CH_3CN to rhodathioborane. *D*-values of 4.29×10^{-9}, 4.34×10^{-9}, and 5.4×10^{-9} m^2/s have been published for acetonitrile.[25] A decrease in the *D*-value is consistent with the interaction of acetonitrile with the polyhedral cluster, which because of its bigger size should have lower *D*-values, slowing down, therefore, the diffusion of the smaller CH_3CN molecules.

dx.doi.org/10.1021/ic301715n | *Inorg. Chem.* 2013, 52, 211−221

The reaction between **3** and carbon monoxide gives **5** in high yield.[2] Related to this reaction, the treatment of **3** with pyridine affords a new rhodathiaborane that has been characterized by multinuclear NMR spectroscopy and mass spectrometry as [8,8,8-(Cl)(Py)(PPh_3)-9-(Py)-*nido*-8,7-$RhSB_9H_9$] (**20**). A comparison of the ^{11}B NMR spectrum shows that the pattern is very similar to those of the CO and bis-PMe_3-ligated adducts, **5** and **13** (Figure 5); and to the monophosphine derivative, **3**.

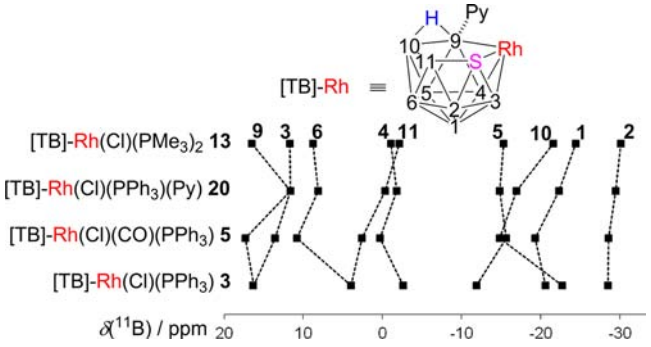

Figure 5. Diagrams representing the chemical shifts in the ^{11}B NMR spectra. Hatched lines connect equivalent positions.

Since shielding patterns provide potential information regarding the cluster bonding, this comparative NMR work suggests that the {η^4-SB_9H_9(Py)}-to-rhodium interaction in the formally unsaturated {RhCl(PR_3)}-ligated species, **3**, **11**, **12**, and **15**, is fundamentally the same than in the saturated {RhCl(PR_3)$_2$}-ligated derivatives, **13**, **14**, and **20**. These species may, therefore, be regarded as sixteen-electron {RhCl(PR_3)} and eighteen-electron {RhCl(PR_3)$_2$} complexes with the {*nido*-SB_9H_9(Py)} moiety, which is acting as a *tetrahapto* ligand with bidentate character: this would imply a basic four-orbital square-planar and five-orbital square-pyramidal metal coordination sphere (see Figure 1).

The ^{31}P-{^1H} NMR spectrum of **20** exhibits a sharp doublet at δ +30.5, suggesting that the PPh_3 ligand of the pyridine adduct remains *trans* to the S(7) vertex. This contrasts to the CO adduct, **5**, which shows a very broad resonance at room temperature, and a configuration in the solid state with the PPh_3 ligand *trans* to the B(9) vertex. Interestingly, the best agreement between the measured ^{11}B NMR chemical shift values and the boron nuclear shielding properties, as calculated via the GIAO approach (Supporting Information, Figures S7–S9, and Table S11), corresponds to the PH_3 model in which the phosphine ligand is *trans* to the S(7) vertex, the pyridine *trans* to the B(3)–B(4) edge, and the chlorine *trans* to the B(9) vertex (Supporting Information, Figure S9).

A general characteristic of boranes, heteroboranes, and their metal derivatives metallaboranes and metallaheteroboranes, is that B–H–B bridging hydrogen atoms are relative acidic. This allows, for example, the deprotonation of polyhedral boron-containing compounds such as *nido*-$B_{10}H_{14}$,[26] *arachno*-4-CB_8H_{14},[27] *arachno*-4-SB_8H_{12},[28] *nido*-4-NB_9H_{12},[11] [8,8-(PPh_3)$_2$-*nido*-8,7-$RhSB_9H_{10}$],[4] or [8,8-(PMe_2Ph)$_2$-*nido*-8,7-$PtB_{10}H_{12}$][29] by treatment with the strong bases. Following this approach, the reaction of the rhodathiaborane, **3**, with the non-nucleophilic base *N*,*N*,*N*′,*N*′-tetramethylnaphthalene-1,8-diamine, commonly known as Proton Sponge (PS), in dichloromethane afforded small amounts of the bis-PPh_3-ligated *closo*-parent cluster, **2**, and the salt [PSH]Cl. However, when the reaction was carried out in the presence of 1 equiv of PPh_3, the reaction is quantitative. Similarly, the treatment of the CO-ligated cluster, **5**, with PS affords the CO-ligated *closo*-cluster, [1,1-(CO)(PPh_3)-3-(Py)-1,2-$RhSB_9H_8$] (**4**).

As summarized in Scheme 3, the reactions of **3** and **5** with PS permit two reaction cycles to be constructed. For both rhodathiaboranes, HCl leads to a *closo*-to-*nido* transformation of the clusters, whereas the PS induces the reverse *nido*-to-*closo* change and the consequent regeneration of **2** and **4**. The reactions are, therefore, connected by HCl addition and [PSH]Cl salt release. If we consider the cycles with species "in" balanced against species "out", the net reactions are eqs 2 and 3:

$$PS + PPh_3 + HCl \rightarrow [PSH]Cl + PPh_3 \quad (2)$$

$$PS + HCl \rightarrow [PSH]Cl \quad (3)$$

These two new stoichiometric cycles are, therefore, driven by simple Brønsted acid/base chemistry.

CONCLUSIONS

The PPh_3-ligated rhodathiaboranes, **1**, **2**, and **4**, react readily with aqueous HCl to give new Cl-ligated clusters in high yields. Similarly, the PR_3-ligated analogues, **6**–**10**, react with hydrochloric acid to give Cl-ligated clusters. In contrast to the PPh_3-counterparts, these reactions are less selective, giving rise to the formation of mixtures that contain [8,8-(Cl)(PR_3)-9-(Py)-*nido*-8,7-$RhSB_9H_9$], where PR_3 = PMe_3 (**11**), PMe_2Ph (**12**), or $PMePh_2$ (**15**), and [8,8,8-(Cl)(PR_3)$_2$-9-(Py)-*nido*-8,7-$RhSB_9H_9$], where PR_3 = PMe_3 (**13**) or PMe_2Ph (**14**). For the {RhCl(PR_3)$_2$}-containing compounds, **13** and **14**, the

Scheme 3

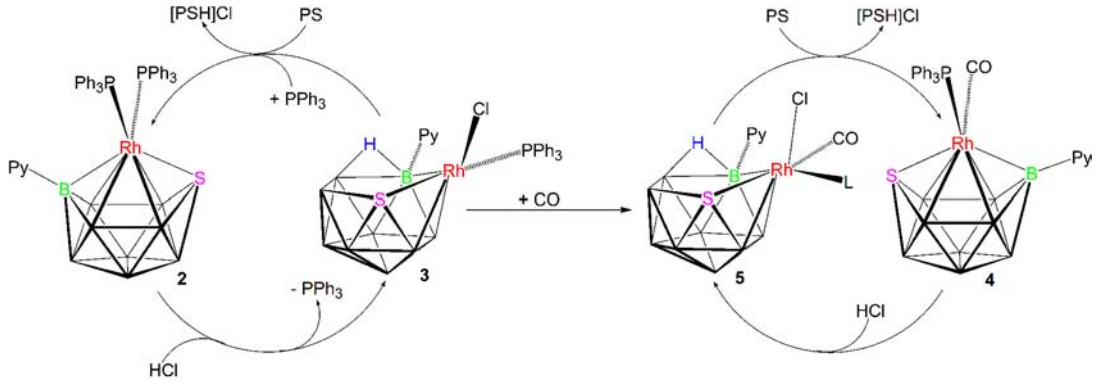

dx.doi.org/10.1021/ic301715n | Inorg. Chem. 2013, 52, 211–221

reaction implies the addition of HCl to the 11-vertex *closo*-clusters and the transformation of the structure to *nido*. This structural opening is consistent with the thesis that the introduction of one electron pair into a *closo* cluster opens the cage to a *nido* framework. However, the formation of the mono-PR_3-ligated species, **3**, **11**, and **12**, from the corresponding *closo*-compounds, takes place with the loss of a phosphine ligand to give formally unsaturated 12 sep clusters with *nido*-structures, rather than the predicted *closo*-isomers. DFT-calculations demonstrate that the *nido*-structure is more stable than the *closo*, without the need to invoke intramolecular Rh···CH agostic interactions.

The unsaturated nature of the mono-PR_3-ligated species, **3**, **11**, **12**, and **15**, is further demonstrated by *(i)* experiments that show interaction between the PPh_3 derivative, **3**, and MeCN in solution, *(ii)* the formation of bis-PR_3-ligated species, **13** and **14**, and *(iii)* the reactions of **3** with carbon monoxide and pyridine that afford the corresponding Rh-CO and Rh-Py adducts, **5** and **20**.

Irrespective of the mechanism, the clusters can accommodate the Brønsted acid, HCl, demonstrating the bifunctional acid/base nature of these 11-vertex rhodathiaboranes. In addition, the use of a weak nucleophile and strong base such as PS, promotes the extrusion of HCl (as the [PSH]Cl salt) from the *nido*-clusters, and their consequent structural transformation to *closo*, closing stoichiometric cycles that are driven by acid/base chemistry (Scheme 3). Sustainable chemical transformations are reliant on reversible processes, based on catalytic and stoichiometric cycles. The *closo*→*nido* interconvertions of 11-vertex rhodathiaboranes via addition/elimination of HCl, are new examples of stoichiometric cycles that may find their way into some synthetic applications. We are exploring these and other aspects arising from the chemistry of these polyhedral clusters.

EXPERIMENTAL SECTION

General Procedures. Reactions were carried out under an argon atmosphere using standard Schlenk-line techniques. Solvents were obtained dried from a Solvent Purification System of Innovative Technology Inc. The 11-vertex rhodathiaboranes **1**, **2**, **4**, **6**, **7**, **8**, **9**, and **10** were prepared according to the literature methods.[1−3] Proton Sponge was purchased from Aldrich and used as received. Preparative thin-layer chromatography (TLC) was carried out using 1 mm layers of silica gel G (Fluka, type GF254) made from water slurries on glass plates of dimensions 20 × 20 cm and dried in air at 25 °C. Infrared spectra were recorded on a Perkin-Elmer Spectrum 100 spectrometer, using a Universal ATR Sampling Accessory. NMR spectra were recorded on Bruker Avance 300-MHz and AV 400-MHz spectrometers, using $^{31}P\{^1H\}$, ^{11}B, $^{11}B\{^1H\}$, ^1H, $^1H\{^{11}B\}$ and $^1H\{^{11}B$(selective)$\}$ techniques. Residual solvent protons were used as reference (δ, ppm, $CDCl_3$, 7.26; CD_2Cl_2, 5.33; CD_3CN, 1.96). ^{11}B chemical shifts are quoted relative to $[BF_3(OEt)_2)]$, and ^{31}P chemical shifts are quoted relative to 85% aqueous H_3PO_4. Mass spectrometric data were recorded on a MICROFLEX instrument operating in either positive or negative modes, using matrix-assisted laser desorption ionization (MALDI). A nitrogen laser of 337 nm (photon energy of 3.68 eV) was used for the ionization processes, and the molecules under study were protected with a matrix of *trans*-2-[3-(4-*tert*-Butylphenyl)-2-methyl-2-propenylidene]malononitrile (DCTB).

Criteria of purity for the Cl-ligated species **11**, **12**, **13**, **14**, and **15** were clean multinuclear NMR spectra allied with mass spectrometric fragmentation patterns.

X-ray crystallography. The structures of **3** and **5** were reported in reference 2. Crystals of compounds **13** and **14** suitable for X-ray diffraction analysis were grown by slow diffusion of hexane into a concentrated solution of each rhodathiaborane in dichloromethane. X-ray diffraction data were collected at low temperature (100(2) K) on an automatic Bruker Kappa APEX DUO CCD area detector diffractometer equipped with graphite-monochromatic Mo−K_α radiation (λ = 0.71073 Å) using narrow frames (0.3° in ω). In all cases, single crystals were mounted on a fiber and were covered with a protective perfluoropolyether. Intensities were integrated including Lorentz and polarization effect with the SAINT-Plus program[30] and corrected for absorption using multiscan methods applied with the SADABS program.[31] The structures were solved using the SHELXS-97 program.[32] Refinements were carried out by full-matrix least-squares on F^2 with SHELXL-97,[33] including isotropic and subsequent anisotropic displacement parameters for all non-hydrogen atoms. Experimental diffraction parameters and crystal data are gathered in Table 3.

Table 3. Crystallographic Data and Structure Refinement Information for 13 and 14

compound	13	14
chemical formula	$C_{14}H_{38}B_9ClNOP_2RhS$	$C_{22}H_{38}B_9Cl_3NP_2RhS$
formula Mass	566.11	717.08
crystal system	monoclinic	orthorhombic
a/Å	24.184(5)	14.6864(11)
b/Å	15.085(3)	16.7403(13)
c/Å	14.588(3)	26.010(2)
α/deg	90.00	90.00
β/deg	93.002(3)	90.00
γ/deg	90.00	90.00
unit cell volume/Å^3	5314.8(18)	6394.8(8)
temperature/K	100(2)	100(2)
space group	*C*2/*c*	*Pbca*
no. of formula units per unit cell, Z	8	8
radiation type	MoK_α	Mo$K\alpha$
absorption coefficient, μ/mm^{-1}	0.951	0.967
no. of reflections measured	28762	83840
no. of independent reflections	6964	6284
R_{int}	0.0220	0.0788
final R_1 values ($I > 2\sigma(I)$)	0.0258	0.0304
final $wR(F^2)$ values ($I > 2\sigma(I)$)	0.0677	0.0672
final R_1 values (all data)	0.0276	0.0531
final $wR(F^2)$ values (all data)	0.0685	0.0725
goodness of fit on F^2	1.130	1.028

Calculations. All calculations were performed using the Gaussian 03 package.[34] Structures were initially optimized using standard methods with the STO-3G* basis-sets for C, B, P, S, and H and with the LANL2DZ basis-set for the rhodium atom. The final optimizations, including frequency analyses to confirm the true minima, together with GIAO nuclear-shielding calculations, were performed using the B3LYP methodology, with the 6-31G* and LANL2DZ basis-sets. The GIAO nuclear shielding calculations were performed on the final optimized geometries, and computed ^{11}B shielding values were related to chemical shifts by comparison with the computed value for B_2H_6, which was taken to be $\delta(^{11}B)$ +16.6 ppm relative to the $BF_3(OEt_2)$ = 0.0 ppm standard.

DOSY experiments. The ^1H DOSY experiments were performed on a Bruker Avance 400 MHz spectrometer. During the DOSY experiments, the temperature was set to 300 K and maintained with an air flow of 400 L h^{-1}. The experiments were acquired with the pulse program, "stebpgp1s", in Bruker software with spinning of the sample to avoid convection influence. The diffusion time (D20) and gradient duration (P30) were optimized with the "stebpgp1s" sequence by

dx.doi.org/10.1021/ic301715n | *Inorg. Chem.* 2013, 52, 211−221

observation of progressive decay of the signal intensities of the acetonitrile peak in CD_2Cl_2 for each measurement until 1 to 5% of the residual signal with maximum strength (95%). The value of D20 employed in the ^1H DOSY experiments was set to 100 ms and the spoil gradient (P19) to 0.6 ms, while P30′ s of 2.5 and 1.2 ms were optimized for a solution of **3** (20.1 mg, 0.033 mmol) in 0.4 mL of CD_2Cl_2 with 6.8 μL of CH_3CN; and for free CH_3CN (in the same molar ratio as in the presence of **3**) in CD_2Cl_2. The gradient strength was varied between 2% and 95% in 16 square spaced increments. AQ = 5.4 s, 8 scans, and a relaxation delay, D1, of 1 were used. The raw data were processed using the Bruker DOSY package and T_1/T_2 relaxation module. The fitting curves for free acetonitrile and acetonitrile in the presence of compound **3** are presented as Supporting Information in Figure S13.

*[8,8-(Cl)(PMe$_3$)-9-(Py)-nido-8,7-RhSB$_9$H$_9$] (**11**).* A solution of [1,1-(PMe$_3$)$_2$-3-(Py)-*closo*-1,2-RhSB$_9$H$_8$] (**9**) (35.4 mg, 0.075 mmol) in dichloromethane was treated with aqueous HCl (37% wt). The reaction mixture was stirred for 30 min at room temperature under argon. Then, the solution was filtered through Celite using a cannula. The resulting orange filtrate was dried over $MgSO_4$ for 2 h. After the removal of the magnesium sulfate, the solvent was evaporated, and the resulting solid washed three times with hexane to give **11** (39.7 mg, 0.064 mmol, 87%). IR (ATR): v 2530 vs (BH). IR (ATR): v 2530 vs (BH). ^{11}B NMR (96 MHz, CD_2Cl_2, 300 K): δ +15.4 (2B, s, BH, B-py), +4.1 (2B, br, BH), +1.4 (1B, d, $^1J_{BH}$ = 131 Hz, BH), −5.1 (1B, d, $^1J_{BH}$ = 141 Hz, BH), −11.7 (1B, d, $^1J_{BH}$ = 135 Hz, BH), −22.5 (1B, d, $^1J_{BH}$ = 144 Hz, BH), −25.4 (1B, d, $^1J_{BH}$ = 116 Hz, BH), −28.7 (1B, br, BH). ^1H-{^{11}B} NMR (300 MHz, $CDCl_3$, 300 K): δ +9.48 (2H, s, H_o-NC_5H_5), +8.20 (1H, m, H_p-NC_5H_5), +7.73 (2H, m, H_m-NC_5H_5), +4.18 (1H, s, BH), +3.41 (1H, s, BH), +3.24 (1H, s, BH), +2.74 (1H, s, BH), +2.64 (1H, s, BH), +1.41 (1H, s, BHB), +1.12 (3H, d, $^2J_{HP}$ = 10.9 Hz, P*Me*$_3$] +0.80 (2H, s, BH). ^{31}P-{^1H} NMR (121 MHz, $CDCl_3$, 300 K): δ +7.8 (d, $^1J_{RhP}$ = 145 Hz). Anal. Calcd. for $C_8H_{23}B_9ClNPRhS\cdot(HCl)$: C, 20.51; H, 5.16; N, 2.99. Found: C, 19.95; H, 5.15; N, 2.69. LRMS (MALDI): *m*/*z* 396 [M$^+$−(Cl+H), isotope envelope. $B_9C_8H_{23}NPRhS$ requires 396; $B_9C_8ClH_{24}NPRhS$ requires 432], 472 [M$^+$+PMe$_3$−(Cl+H), isotope envelope. $B_9C_{11}H_{31}NPRhS$ requires 472].

*[8,8-(Cl)(PMe$_2$Ph)-9-(Py)-nido-8,7-RhSB$_9$H$_9$] (**12**).* A solution of [1,1-(PMe$_2$Ph)$_2$-3-(Py)-*closo*-1,2-RhSB$_9$H$_8$] (**10**) (20 mg, 0.034 mmol) in dichloromethane was treated with aqueous HCl (37% wt). The reaction mixture was stirred for 2 h at room temperature under argon. Then, the solution was filtered through Celite using a cannula. The resulting orange filtrate was dried over $MgSO_4$ for 2 h. After the removal of the magnesium sulfate, the solvent was evaporated, and the resulting solid washed three times with hexane to give **12** (11 mg, 0.021 mmol, 64%). ^{11}B-{^1H} NMR (128 MHz; CD_2Cl_2; 298 K): δ +14.9 (2B, s, B-py, BH), +1.9 (2B, br, BH), −11.8 (1B, d, $^1J_{BH}$ = 124 Hz, BH), −22.8 (1B, d, $^1J_{BH}$ = 157 Hz, BH), −24.9 (1B, br, BH), −28.5 (1B, br, BH). ^1H-{^{11}B} NMR (400 MHz; CD_2Cl_2; 298 K): δ +8.86 (2H, s, H_o-NC_5H_5), +8.14 (1H, t, $^3J_{HH}$ = 7.6 Hz, H_p-NC_5H_5), +7.55 (2H, t, H_m-NC_5H_5), +7.39 to 7.30 (5H, m, PMe$_2$*Ph*), +4.22 (1H, s, BH), +3.32 (1H, s, BH), +3.18 (1H, s, BH), +2.92 (1H, s, BH), +2.54 (1H, s, BH), +1.77(1H, s, BHB), +1.67 (3H, br, P*Me*$_2$Ph), +1.58 (3H, d, $^2J_{HP}$ = 10.2 Hz, P*Me*$_2$Ph), +1.22 (1H, s, BH), +0.74 (1H, s, BH). ^{31}P-{^1H} NMR (161 MHz; CD_2Cl_2; 193 K): δ +15.7 ($^1J_{RhP}$ = 140 Hz). LRMS (MALDI): *m*/*z* 458 [M$^+$−(Cl+H), isotope envelope. $B_9C_{13}ClH_{25}NPRhS$ requires 494], 596 [M$^+$+(PMe$_2$Ph)−(Cl+H), isotope envelope. $B_9C_{21}H_{35}NP_2RhS$ requires 596].

*[8,8,8-(Cl)(PMe$_3$)$_2$-9-(Py)-nido-8,7-RhSB$_9$H$_9$] (**13**).* Five milligrams of **9** (0.011 mmol) was dissolved in 0.3 mL of $CDCl_3$ in a 5 mm NMR tube, and then 0.2 mL of HCl (37% wt) was added. The resulting red solution was examined by NMR spectroscopy at room temperature. The NMR data corresponded to **11**; however, evaporation of the $CDCl_3$ solvent and washing (three times) with hexane, afforded an orange solid that showed the mono-PMe$_3$-ligated cluster, **11**, together with the bis-PMe$_3$-ligated derivative, **13** in a 1:1.3 relative intensity ratio, respectively. The ^{11}B-{^1H} NMR spectrum showed overlapping resonances that made difficult the assignment of the resonances among the two Cl-ligated clusters. Of these, the following may be individually assigned to **13**: IR (ATR): v 2522 vs (BH), 1069 m 945 s.^{11}B NMR (96 MHz, CD_2Cl_2, 300 K): δ +12.9 (1B, s, B-Py), +11.7 (1B, br, BH), +5.8 (1B, d, $^1J_{BH}$ = 136 Hz, BH), −1.1 (1B, d, $^1J_{BH}$ = 108 Hz, BH), −2.1 (1B, d, $^1J_{BH}$ = 122 Hz, BH), −15.3 (1B, d, $^1J_{BH}$ = 134 Hz, BH), −21.6 (1B, d, $^1J_{BH}$ = 128 Hz, BH), −24.4 (1B, d, $^1J_{BH}$ = 142 Hz, BH), −30.1 (1B, d, $^1J_{BH}$ = 142 Hz, BH). ^1H-{^{11}B} NMR (300 MHz, CD_2Cl_2, 300 K): δ +9.48 (2H, s, H_o-NC_5H_5), +8.20 (1H, m, H_p-NC_5H_5), +7.73 (2H, m, H_m-NC_5H_5), +3.90 (1H, s, BH), +3.55 (1H, s, BH), +3.08 (1H, s, BH), +3.02 (1H, s, BH), +2.20 (1H, s, BH), 1.66 (1H, s, BHB), +1.40 (3H, d, $^2J_{HP}$ = 8.4 Hz, P*Me*$_3$] +0.96 (2H, s, BH), +0.96 (3H, d, $^2J_{HP}$ = 11.8 Hz, P*Me*$_3$]. ^{31}P-{^1H} RMN (161 MHz, CD_2Cl_2, 183 K): δ −2.2 (1P, dd, $^1J_{RhP}$ = 131 Hz, $^2J_{PP}$ = 28 Hz, PMe$_3$), −24.2 (1P, br. d, $^1J_{RhP} \approx$ 86 Hz, PMe$_3$). LRMS: *m*/*z* (MALDI) 473 [M$^+$-Cl isotope envelope $B_9C_9H_{32}NP_2RhS$; $B_9C_9ClH_{32}NP_2RhS$ requires 508].

*[8,8,8-(Cl)(PMe$_2$Ph)$_2$-9-(Py)-nido-8,7-RhSB$_9$H$_9$] (**14**).* Eight milligrams of **10** (0.012 mmol) was dissolved in 0.3 mL of $CDCl_3$ in a 5 mm NMR tube, and then 0.2 mL of HCl (37% wt) was added. The resulting red solution was examined by NMR spectroscopy at room temperature. The NMR data corresponded to the above-characterized chloro-ligated derivative **12**; however, evaporation of the $CDCl_3$ solvent and washing (three times) with hexane, afforded an orange solid that showed the mono-PMe$_2$Ph-ligated cluster, **12**, and the *bis*-PMe$_2$Ph-ligated derivative, **14**, in a 0.3:1 relative intensity ratio, respectively. The ^{11}B-{^1H} NMR spectrum showed overlapping resonances that made difficult the assignment of the resonances among the two Cl-ligated clusters. Of these, the following may be individually assigned to **14**: ^{11}B-{^1H} NMR (96 MHz, CD_2Cl_2, 300 K): δ +12.4 (1B, s, B-Py), +8.3 (1B, br, BH), +2.7 (1B, d, $^1J_{BH}$ = 117 Hz, BH), −3.0 (1B, d, $^1J_{BH}$ = 119 Hz, BH), −11.5 (1B, d, $^1J_{BH}$ = 137 Hz, BH), −13.3 (1B, br, BH), −18.1(1B, d, $^1J_{BH}$ = 139 Hz, BH), −22.0 (1B, d, $^1J_{BH}$ = 148 Hz, BH), −29.5 (1B, br, BH). ^1H-{^{11}B} NMR (300 MHz; CD_2Cl_2; 298 K): (300 MHz, CD_2Cl_2, 300 K): δ +9.48 (2H, s, H_o-NC_5H_5), +8.06 (1H, m, H_p-NC_5H_5), +7.74 (2H, m, H_m-NC_5H_5), +7.51 to 7.05 (10H, m, PMe$_2$Ph), +3.92 (1H, s, BH), +3.70 (1H, s, BH), +2.90 (1H, s, BH), +2.72 (1H, s, BH), +1.94 (1H, s, BH), +1.65 (3H, d, $^2J_{HP}$ = 8.9 Hz, P*Me*$_2$Ph) +1.58 (1H, s, BHB), +1.44 (3H, d, $^2J_{HP}$ = 8.2 Hz, P*Me*$_2$Ph), +1.00 (1H, s, BH), +0.92 (3H, d, $^2J_{HP}$ = 10.6 Hz, P*Me*$_2$Ph), +0.65 (3H, d, $^2J_{HP}$ = 9.3 Hz, P*Me*$_2$Ph), +0.28 (1H, s, BH). ^{31}P-{^1H} NMR (161 MHz, CD_2Cl_2, 183 K): δ +8.4 (1P, d, $^1J_{RhP}$ = 140 Hz, $^2J_{PP}$ = 26 Hz), −17.3 (1P, d, $^1J_{RhP}$ = 78 Hz). LRMS: *m*/*z* (MALDI) 596 [M$^+$−(Cl+H), isotope envelope. $B_9C_{21}H_{35}NP_2RhS$ requires 596; $B_9C_{21}ClH_{36}NP_2RhS$ requires 632].

*[8,8-(Cl)(PMePh$_2$)-9-(Py)-nido-8,7-RhSB$_9$H$_9$] (**15**).* A solution of [8,8,8-H(PMePh$_2$)$_2$-9-(Py)-*nido*-8,7-RhSB$_9$H$_9$] (**6**) (30 mg, 0.041 mmol) in dichloromethane was treated with aqueous HCl (37% wt). The reaction mixture was stirred for 2 h at room temperature under argon. Then, the solution was filtered through Celite using a cannula. The resulting orange filtrate was dried over $MgSO_4$ for 2 h. After the removal of the magnesium sulfate, the solvent was evaporated and the resulting solid washed three times with hexane to give **15** (12.2 mg, 0.022 mmol, 53%). IR (ATR): v 2524 vs (BH), 1259 m, 1017 m, 797 s, 691 s. ^{11}B-{^1H} NMR (96 MHz; CD_2Cl_2; 298 K): δ +15.2 (2B, s, BH, B-py), +2.6 (2B, d, $^1J_{BH}$ = 140 Hz, BH), −4.1 (1B, d, $^1J_{BH}$ = 120 Hz, BH), −12.2 (1B, d, $^1J_{BH}$ = 148 Hz, BH), −22.3 (1B, d, $^1J_{BH}$ = 151 Hz, BH), −23.9 (1B, d, $^1J_{BH}$ = 140 Hz, BH), −29.2 (1B, br, BH). ^1H-{^{11}B} NMR (300 MHz; CD_2Cl_2; 298 K): δ +8.59 (2H, m, H_o-NC_5H_5), +7.94 (1H, m, H_p-NC_5H_5), +7.60 (2H, m, H_m-NC_5H_5), +7.54 to 6.95 (10H, m, P*Me*Ph$_2$), +4.71 (1H, s, BH), +4.33 (1H, s, BH), +3.45 (1H, s, BH), +3.03 (1H, s, BH),+1.81 (1H, s, BH), +1.79 (3H, d, $^2J_{HP}$ = 10.2 Hz, P*Me*Ph$_2$), +1.13 (1H, s, BHB). ^{31}P-{^1H} NMR (161 MHz; CD_2Cl_2; 300 K): δ +18.1 (1P, d, $^1J_{RhP}$ = 149 Hz). Anal. Calcd. for $C_{18}H_{27}B_9ClNPRh$: C, 38.88; H, 4.89; N, 2.52. Found: C, 38.95; H, 4.25; N, 1.57. LRMS (MALDI): *m*/*z* 554 [M−(H), isotope envelope. $B_9C_{18}ClPH_{26}NRhS$ requires 554; $B_9C_{21}ClH_{27}NP_2RhS$ requires 556], 520 [M−(Cl+H), isotope envelope. $B_9C_{18}PH_{26}NRhS$ requires 520; $B_9C_{21}ClH_{27}NP_2RhS$ requires 556]. HRMS (MALDI): *m*/*z* calc. for $B_9C_{18}ClPH_{26}NRhS$ 554.1075, found 554.1051. HRMS (MALDI): *m*/*z* calc. for $B_9C_{18}PH_{26}NRhS$ 521.1415, found 521.1432.

dx.doi.org/10.1021/ic301715n | *Inorg. Chem.* 2013, 52, 211−221

*[8,8,8-(Cl)(Py)(PPh$_3$)-9-(Py)-nido-8,7-RhSB$_9$H$_9$] (**20**).* 14.3 mg of **3** (0.023 mmoL) was dissolved in 10 mL of CH_2Cl_2 in a Schlenk tube, and then 7.48 μL (7.32 mg, 0.093 mmoL) of pyridine was added to the orange solution in dichloromethane (10 mL). The solvent was evaporated, and the resulting solid washed three times with hexane to give **20** (9.8 mg, 0.014 mmol, 61%). ^{11}B NMR (128 MHz, $CDCl_3$, 300 K): δ +11.6 (2B, br, BH, B-Py), +8.1 (1B, br, BH), −0.3 (1B, br, BH), −1.8 (1B, br, BH), −14.8 (1B, d, $^1J_{BH}$ = 142 Hz, BH), −16.9 (1B, d, $^1J_{BH}$ = 125 Hz, BH), −22.3 (1B, d, d, $^1J_{BH}$ = 125 Hz, BH), −29.5 (1B, br, BH). ^{1}H-{^{11}B} NMR (400 MHz, $CDCl_3$, 300 K): δ +8.82 (2H, d, $^3J_{HH}$ = 8.8 Hz, H_o-NC_5H_5−B), +8.71 (2H, br, H_o-NC_5H_5−Rh), 7.97 (1H, br, H_p-NC_5H_5−Rh), +7.83 (1H, t, $^3J_{HH}$ = 7.7 Hz, H_p-NC_5H_5−B), +7.58 (2H, t, $^3J_{HH}$ = 7.7 Hz, H_m-NC_5H_5−B), +7.50−7.06 (15H, m, PPh_3), +3.94 (1H, s, BH), +3.81 (1H, s, BH), +3.76 (1H, s, BH), +3.00 (1H, s, BH), +2.89 (1H, s, BH), +2.06 (1H, s, BH), +1.86 (1H, s, BH), +1.75 (1H, s, BHB). ^{31}P-{^{1}H} NMR (161 MHz, $CDCl_3$, 300 K): δ +30.5 (d, $^1J_{RhP}$ = 146 Hz).

*Reaction of [1,1-(PPh$_3$)(PMe$_3$)-3-(Py)-closo-1,2-RhSB$_9$H$_8$] (**8**) with HCl.* Five milligrams (0.0076 mmol) of **8** was dissolved in 0.3 mL of CD_2Cl_2 in a 5 mm NMR tube, and was treated with aqueous HCl (37% wt). The resulting solution was examined by NMR spectroscopy at room temperature. The NMR data revealed the formation of the Cl-ligated monophosphine rhodathiaboranes, [8,8-(Cl)(PPh_3)-9-(Py)-*nido*-8,7-$RhSB_9H_9$] (**3**) and [8,8-(Cl)(PMe_3)-9-(Py)-*nido*-8,7-$RhSB_9H_9$] (**11**) in a 1:2 ratio, respectively.

*[8,8,8-(H)(PMe$_3$)(PPh$_3$)-9-(Py)-nido-8,7-RhSB$_9$H$_9$] (**7**) with HCl.* A solution of **7** (13.7 mg, 0.021 mmol) in dichloromethane was treated with aqueous HCl (37% wt). The reaction mixture was stirred for 2 h at room temperature under argon. Then, the solution was filtered through Celite using a cannula. The resulting orange filtrate was dried over $MgSO_4$ for 2 h. After the removal of the magnesium sulfate, the solvent was evaporated, and the resulting solid washed three times with hexane. NMR spectroscopy showed that the solid was mainly compound **3**, together with small amounts of unidentified species.

*Study of the Interaction of **3** with MeCN.* 5.5 mg of **3** (0.0089 mmol) was dissolved in 0.3 mL of $CDCl_3$ in a 5 mm NMR tube, and then 4 μL of CH_3CN (0.076 mmol) was added to the orange solution. The resulting solution was examined by NMR spectroscopy at room temperature. ^{11}B NMR (96 MHz, $CDCl_3$, 300 K): δ +14.9 (2B, broad, BH, B-Py), +4.9 (1B, d, $^1J_{BH}$ = 132 Hz, BH), +2.5 (1B, broad, BH), −2.1 (1B, d, $^1J_{BH}$ = 107 Hz, BH), −13.5 (1B, d, $^1J_{BH}$ = 137 Hz, BH), −21.3 (1B, d, $^1J_{BH}$ = 130 Hz, BH), −29.2 (1B, broad, BH). ^{1}H-{^{11}B} NMR (300 MHz, $CDCl_3$, 300 K): δ +8.83 (1H, m, H_o-NC_5H_5), +7.91 (1H, m, H_p NC_5H_5), +7.42 (2H, m, H_m NC_5H_5), +7.39−7.28 (15H, m, PPh_3), +4.58 (1H, s, BH), +3.55 (1H, s, BH), +3.23 (1H, s, BH), +2.96 (1H, s, BH),+2.71 (1H, s, BH), +1.96 (1H, s, BH), +1.71 (1H, s, BHB), +1.23 (1H, s, BH), +1.04 (1H, s, BH). ^{31}P-{^{1}H} NMR (121 MHz, $CDCl_3$, 300 K): δ +32.1 (1P, d, $^1J_{RhP}$ = 149 Hz).

Supporting Information, Figures S10 to S12 illustrate the variation of the ^{11}B-{^{1}H}, ^{1}H-{^{11}B}, and ^{31}P-{^{1}H} NMR spectra of **3** in $CDCl_3$ in the presence of different amounts of free acetonitrile, and in neat CD_3CN. The NMR data in CD_3CN is as follow: ^{11}B NMR (160 MHz, 300 K): δ +14.9 (minor, 1B, s, B-py), +12.1 (1B, s, B-py), +7.6 (1B, d, $^1J_{BH}$ = 135 Hz, BH), +4.9 (minor, 1B, d, $^1J_{BH}$ = 119 Hz, BH), +0.1 (1B, d, $^1J_{BH}$ = 133 Hz, BH), −2.6 (1B, d, $^1J_{BH}$ = 126 Hz, BH), −16.6 (1B, d, $^1J_{BH}$ = 140 Hz, BH), −18.6 (1B, d, $^1J_{BH}$ = 113 Hz, BH), −22.0 (1B, d, $^1J_{BH}$ = 135 Hz, BH), −22.9 (1B, d, $^1J_{BH}$ = 141 Hz, BH), −29.9 (1B, d, $^1J_{BH}$ = 107 Hz, BH). ^{1}H-{^{11}B} NMR (500 MHz, 300 K): δ +8.95 (2H, m, H_o NC_5H_5), +8.25 (1H, m, H_p NC_5H_5), +7.90 (2H, m, H_m NC_5H_5), +7.53−7.18 (15H, m, PPh_3),+4.20 (1H, s, BH), +3.84 (minor, 1H, s, BH), +3.61 (1H, s, BH), +3.49 (1H, s, BH), +2.94 (1H, s, BH), +1.80 (1H, s, BH), +1.15 (1H, s, BH), +1.02 (1H, s, BH), +0.60 (1H, s, BH). ^{31}P-{^{1}H} NMR (202 MHz, 300 K): δ +32.4 (d, $^1J_{RhP}$= 143 Hz, PPh_3), +15.54 (minor, 1P, s, PPh_3), ratio 1:0.23.

*Reaction of [8,8-(Cl)(PPh$_3$)-9-(Py)-nido-8,7-RhSB$_9$H$_9$] (**3**) with Proton Sponge (PS).* 7.1 mg of **3** (0.012 mmol) was dissolved in 0.3 mL of CD_2Cl_2 in a 5 mm NMR tube together with stoichiometric amounts of free PPh_3; then 2.50 mg of Proton Sponge (0.012 mmol) was added to the orange solution. The resulting reaction mixture was examined by NMR spectroscopy at room temperature. The NMR data demonstrated the quantitative formation of the parent *closo*-compound, [1,1-(PPh_3)$_2$-3-(Py)-*closo*-1,2-$RhSB_9H_8$] (**2**), together with the [PSH]Cl salt. ^{1}H-{^{11}B} NMR data for [PSH]Cl (400 MHz; CD_2Cl_2; 298 K): δ 18.68 (1H, s, $H^+N_2C_{14}H_{18}$), 7.94 (2H, m, Ho-$H^+N_2C_{14}H_{18}$), 7.75 (2H, m, Hp-$H^+N_2C_{14}H_{18}$), 7.65 (1H, m, Hm-$H^+N_2C_{14}H_{18}$), 3.23 (12H, s, CH_3- $H^+N_2C_{14}H_{18}$).

*Reaction of [8,8,8-(Cl)(CO(PPh$_3$)-9-(Py)-nido-8,7-RhSB$_9$H$_9$] (**5**) with Proton Sponge (PS).* An NMR tube was charged with 6.3 mg (0.01 mmol) of **5**, which was dissolved in 0.3 mL of CD_2Cl_2. Then, 2.5 mg (0.012 mmol) of PS was added to the solution under an argon atmosphere. The reaction was shaken 5 min at room temperature, and studied by NMR. The spectroscopic data demonstrated the quantitative formation of the parent *closo*-compound, [1,1-(CO)-(PPh_3)-3-(Py)-*closo*-1,2-$RhSB_9H_8$] (**4**), together with the [PSH]Cl salt.

■ ASSOCIATED CONTENT

Ⓢ Supporting Information

DFT-calculated NMR data; spectra of **3** in the presence of CH_3CN; DOSY experiments; and cif files for **13** and **14**. This material is available free of charge via the Internet at http://pubs.acs.org.

■ AUTHOR INFORMATION

Corresponding Author

*E-mail: rmacias@unizar.es.

Notes

The authors declare no competing financial interest.

■ ACKNOWLEDGMENTS

We acknowledge the Spanish Ministry of Science and Innovation (CTQ2009-10132, CONSOLIDER INGENIO, CSD2009-00050, MULTICAT and CSD2006-0015, Crystallization Factory) for support of this work. B.C. thanks the "Diputación General de Aragón" for a predoctoral scholarship.

■ REFERENCES

(1) (a) Álvarez, A.; Macías, R.; Fabra, M. J.; Lahoz, F. J.; Oro, L. A. *J. Am. Chem. Soc.* **2008**, *130*, 2148. (b) Álvarez, A.; Macías, R.; Bould, J.; Fabra, M. J.; Lahoz, F. J.; Oro, L. A. *J. Am. Chem. Soc.* **2008**, *130*, 11455.

(2) Calvo, B.; Macías, R.; Cunchillos, C.; Lahoz, F. J.; Oro, L. A. *Organometallics* **2012**, *31*, 2526.

(3) Calvo, B.; Álvarez, Á.; Macías, R.; García-Orduña, P.; Lahoz, F. J.; Oro, L. A. *Organometallics* **2012**, *31*, 2986.

(4) Ferguson, G.; Jennings, M. C.; Lough, A. J.; Coughlan, S.; Spalding, T. R.; Kennedy, J. D.; Fontaine, X. L. R.; Stibr, B. *J. Chem. Soc., Chem. Commun.* **1990**, 891.

(5) Macías, R.; Rath, N. P.; Barton, L. *Organometallics* **1999**, *18*, 3637.

(6) Álvarez, A.; Macías, R.; Bould, J.; Cunchillos, C.; Lahoz, F. J.; Oro, L. A. *Chem.—Eur. J.* **2009**, *15*, 5428.

(7) Murphy, M.; Spalding, T. R.; Ferguson, G.; Gallagher, J. F. *Acta Crystallogr., Sect. C: Cryst. Struct. Commun.* **1992**, *C48*, 638.

(8) Rosair, G. M.; Welch, A. J.; Weller, A. S. *Acta Crystallogr.* **1996**, *C52*, 3020.

(9) Bould, J.; Cunchillos, C.; Lahoz, F. J.; Oro, L. A.; Kennedy, J. D.; Macías, R. *Inorg. Chem.* **2010**, *49*, 7353.

(10) Nestor, K.; Fontaine, X. L. R.; Greenwood, N. N.; Kennedy, J. D.; Plešek, J.; Štíbr, B.; Thornton-Pett, M. *Inorg. Chem.* **1989**, *28*, 2219.

(11) Macías, R.; Bould, J.; Holub, J.; Kennedy, J. D.; Štíbr, B.; Thornton-Pett, M. *Dalton Trans.* **2007**, 2885.

(12) Štíbr, B.; Jelinek, T.; Kennedy, J. D.; Fontaine, X. L. R.; Thornton-Pett, M. *J. Chem. Soc., Dalton Trans.* **1993**, 1261.

(13) Adams, K. J.; McGrath, T. D.; Rosair, G. M.; Weller, A. S.; Welch, A. J. *J. Organomet. Chem.* **1998**, *550*, 315.

(14) Ferguson, G.; Lough, A. L.; Coughlan, S.; Spalding, T. R. *Acta Crystallogr., Sect. C: Cryst. Struct. Commun.* **1992**, *C48*, 440.
(15) Álvarez, A.; Macías, R.; Fabra, M. J.; Martín, M. L.; Lahoz, F. J.; Oro, L. A. *Inorg. Chem.* **2007**, *46*, 6811.
(16) Murphy, M. P.; Spalding, T. R.; Cowey, C.; Kennedy, J. D.; Thornton-Pett, M.; Holub, J. *J. Organomet. Chem.* **1998**, *550*, 151.
(17) Volkov, O.; Rath, N. P.; Barton, L. *Organometallics* **2002**, *21*, 5505.
(18) (a) Wade, K. *Adv. Inorg. Chem. Radiochem.* **1976**, *18*, 1. (b) Williams, R. E. *Adv. Inorg. Chem. Radiochem.* **1976**, *18*, 67.
(19) Evans, D. G.; Mingos, D. M. P. *J. Organomet. Chem.* **1982**, *240*, 321.
(20) (a) Kennedy, J. D. In *The Borane-Carborane-Carbocation Continuum*; Casanova, J., Ed.; Wiley: New York, 1998. (b) Bould, J.; Cooke, P. A.; Dorfler, U.; Kennedy, J. D.; Barton, L.; Rath, N. P.; Thornton-Pett, M. *Inorg. Chim. Acta* **1999**, *285*, 290.
(21) (a) Mingos, D. M. P.; Forsyth, M. I.; Welch, A. J. *J. Chem. Soc., Dalton Trans.* **1978**, 1363. (b) McAnaw, A.; Scott, G.; Elrick, L.; Rosair, G. M.; Welch, A. J. *Dalton Trans.* **2012**, Advance Article, 10.1039/C2DT31515G.
(22) Macías, R.; Holub, J.; Kennedy, J. D.; Stibr, B.; Thornton-Pett, M. *J. Chem. Soc., Chem. Commun.* **1994**, 2265.
(23) Nestor, K.; Kennedy, J. D.; Thornton-Pett, M.; Holub, J.; Štíbr, B. *Inorg. Chem.* **1992**, *31*, 3339.
(24) Bould, J.; Rath, N. P.; Barton, L. *Organometallics* **1996**, *15*, 4916.
(25) Kato, H.; Saito, T.; Nabeshima, M.; Shimada, K.; Kinugasa, S. *J. Magn. Reson.* **2006**, *180*, 266.
(26) Little, J. L.; Wong, A. C. *J. Am. Chem. Soc.* **1971**, *93*, 522.
(27) Kadlecek, D. E.; Sneddon, L. G. *Inorg. Chem.* **2002**, *41*, 4239.
(28) (a) Baše, K.; Wallbridge, M. G. H.; Fontaine, X. L. R.; Greenwood, N. N.; Jones, J. H.; Kennedy, J. D.; Štíbr, B. *Polyhedron* **1989**, *8*, 2089. (b) Luaces, S.; Bould, J.; Macías, R.; Sancho, R.; García-Orduña, P.; Lahoz, F. J.; Oro, L. A. *J. Organomet. Chem.* **2012**, *722*, 22−30.
(29) Bould, J.; Kilner, C. A.; Kennedy, J. D. *Dalton Trans.* **2005**, 1574.
(30) Otwinowski, Z.; Minor, W. In *Methods in Enzymology*; Carter, C. W., Jr., Sweet, R. M., Ed.; Academic Press: New York, 1997; Vol. *276*.
(31) Blessing, R. H. *Acta Crystallogr.* **1995**, *A51*, 33.
(32) Sheldrick, G. M. *Acta Crystallogr.* **1997**, *A46*, 467.
(33) Sheldrick, G. M. *Acta Crystallogr.* **2008**, *A64*, 112.
(34) Frisch, M. J.; Trucks, G. W.; Schlegel, H. B.; Scuseria, G. E.; Robb, M. A.; ; Cheeseman, J. R.; Jr., J., A. M.; Vreven, T.; Kudin, K. N.; Burant, J. C.; J. M..Millam; Iyengar, S. S.; Tomasi, J.; Barone, V.; Mennucci, B.; ; Cossi, M.; Scalmani, G.; Rega, N.; Petersson, G. A.; Nakatsuji, H.; Hada, M.; Ehara, M.; Toyota, K.; Fukuda, R.; Hasegawa, J.; Ishida, M.; Nakajima, T.; Honda, Y.; Kitao, O.; Nakai, H.; Klene, M.; Li, X.; Knox, J. E.; Hratchian, H. P.; Cross, J. B.; Bakken, V.; Adamo, C.; Jaramillo, J.; ; Gomperts, R.; Stratmann, R. E.; Yazyev, O.; Austin, A. J.; Cammi, R.; ; Pomelli, C.; Ochterski, J.; Ayala, P. Y.; Morokuma, K.; Voth, G. A.; Salvador, P.; Dannenberg, J. J.; Zakrzewski, V. G.; Dapprich, S.; Daniels, A. D.; Strain, M. C.; Farkas, O.; Malick, D. K.; Rabuck, A. D.; Raghavachari, K.; Foresman, J. B.; Ortiz, J. V.; Cui, Q.; Baboul, A. G.; Clifford, S.; Cioslowski, J.; Stefanov, B. B.; Liu, G.; Liashenko, A.; Piskorz, P.; ; Komaromi, I.; L.Martin, R.; Fox, D. J.; Keith, T.; Al-Laham, M. A.; Peng, C. Y.; Nanayakkara, A.; Challacombe, M.; Gill, P. M. W.; Johnson, B. G.; Chen, W.; Wong, M. W.; Gonzalez, C.; Pople, J. A. *Gaussian 03*; Gaussian, Inc: Wallingford, CT, 2004.